Structure and Dynamics of a Confined Ionic Liquid. Topics of Relevance to Dye-Sensitized Solar Cells

Carlos Pinilla,[†] Mario G. Del Pópolo,[†] Ruth M. Lynden-Bell,[‡] and Jorge Kohanoff*[,†]

Atomistic Simulation Centre, School of Mathematics and Physics, Queen's University, Belfast BT7 1NN, United Kingdom, and University Chemical Laboratory, Lensfield Road, Cambridge University, Cambridge CB2 1EW, United Kingdom

Received: June 6, 2005; In Final Form: July 22, 2005

The behavior of a model ionic liquid (IL) confined between two flat parallel walls was studied at various interwall distances using computer simulations. The results focus both on structural and dynamical properties. Mass and charge density along the confinement axis reveal a structure of layers parallel to the walls that leads to an oscillatory profile in the electrostatic potential. Orientational correlation functions indicate that cations at the interface orient tilted with respect to the surface and that any other orientational order is lost thereafter. The diffusion coefficients of the ions exhibit a maximum as a function of the confinement distance, a behavior that results from a combination of the structure of the liquid as a whole and a faster molecular motion in the vicinity of the walls. We discuss the relevance of the present results and elaborate on topics that need further attention regarding the effects of ILs in the functioning of IL-based dye-sensitized solar cells.

1. Introduction

Dye-sensitized solar cells (DSSCs) are photovoltaic devices with promising applications in the production of clean and self-sustained energy. These novel solar cells, also known as Grätzel cells, are formed by a layer of a nanocrystalline semiconductor, often TiO_2, impregnated with a dye substance and confined between two transparent electrodes. The microporous structure generated by the semiconductor is embedded in a solution that contains a redox couple, for example, I^-/I_3^-, which is the liquid also in contact with one of the electrodes (cathode).[1−4] The functional principle of the cell is based on the excitation of the dye by incoming sunlight photons. The excited dye injects an electron into the conduction band of the semiconductor, which diffuses through the nanoparticle network to reach the anode.[5−7] The electronic injection leaves the dye in a cationic form that has to be regenerated by the redox couple to maintain a sustained current. The oxidized component of the redox system migrates then through the solution up to the cathode where it is finally reduced and the cycle is closed.

Different organic solvents have been tested in the manufacture of DSSCs,[8−10] although, as a result of problems of evaporation and leaking, most of them deteriorate the performance of the cell after some time of operation. Recently, ionic liquids (ILs) have been proposed as an alternative in the design of DSSCs. Their appealing features are high viscosities and low vapor pressures that minimize leaking and solvent losses, together with high conductivity values and a peculiar screening capacity.

ILs are fluids composed solely of ions that melt in the range of −90 to 200 °C. They are formed by large organic cations combined with different inorganic anions.[11,12] It is known that, as a result of using ILs, the efficiency of a DSSC may be lower than with other organic solvents; however, the long-term stability and performance of the whole device is better.[1,9]

Several factors undermine the efficiency of a DSSC. Loss factors are, for example, recombination processes between the injected electrons and the redox system, the cationic form of the dye, or even the cations of the IL.[15,16] These processes occur in the contact region between the semiconductor and the solution. On the other hand, the motion of the redox components from and to the counter electrode is hindered by the high viscosity of the IL and the diffusion through the disordered porous structure left by the nanoparticles. The estimated diameter of the pores, once coated with the dye, is of the order of 1 nm,[17] so ionic diffusion through these channels can be a limiting factor in the production of current.

As a result of finite size effects and anisotropic forces, a confined fluid can show widely different properties in comparison to the unconstrained liquid.[18−21] In the context of DSSCs, the theory of confined liquids is important to describe the behavior of the ions trapped between the semiconductor grains. Essentially, ionic mobility under confinement is likely to be a major factor in determining the electric current flowing through the DSSC.

The objective of this work is to describe the behavior of a model IL confined between two parallel walls, focusing on confinement effects on the structure and dynamics of the ions, and its impact on the charge-transport capacity. The paper is organized as follows: section 2 describes the simulation methods, section 3 describes and discusses the effects of confinement on the structure and diffusion in the molten salt 1,3-dimethylimidazolium chloride ([DMIM][Cl]), and section 4 contains our conclusions and some remarks in relation to actual DSSCs.

2. Computational Methods

The $[DMIM^+]$ cation, shown in Figure 1, was treated as a rigid 10-site body with united methyl groups. Partial charges

* Corresponding author. Tel.: ++44 (2890) 973770. Fax: ++44 (2890) 975359. E-mail: j.kohanoff@qub.ac.uk.
[†] Queen's University.
[‡] Cambridge University.

10.1021/jp052999o CCC: $30.25
Published on Web 09/01/2005

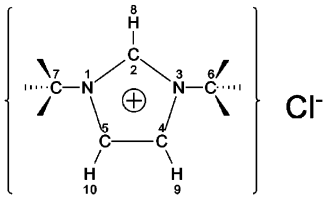

Figure 1. [DMIM][Cl]. A rigid 10-site model with united methyl groups was used in the simulations.

were assigned to these sites according to the values reported in our previous work,[14] while dispersion interactions were modeled by Lennard-Jones potentials using the parameters reported by de Andrade et al.[22]

The model system consisted of 252 ion pairs placed in a hexagonal prismatic box. Molecules were confined between two parallel structureless walls located perpendicular to the principal axis of the cell (direction *Z*). Electrostatic interactions were calculated using the Ewald method, with a real-space cutoff of 17 Å. To take advantage of the greater efficiency of the three-dimensional Ewald sum, periodic boundary conditions were applied in all three directions, with a large dimension in the *Z* direction being used to emulate a semi-infinite slab geometry. The short-range forces were also computed with a cutoff of 17 Å.

The interaction between the molecules and the walls was modeled by an integrated Lennard-Jones potential of the form[23]

$$V_{\mathrm{wall}}(z) = \frac{2\pi\sigma_{\mathrm{w}}{}^3\epsilon_{\mathrm{w}}\rho}{3}\left\{\frac{2}{15}\left(\frac{\sigma_{\mathrm{w}}}{z}\right)^9 - \left(\frac{\sigma_{\mathrm{w}}}{z}\right)^3\right\} \qquad (1)$$

where $\sigma_{\mathrm{w}} = 3.0$ Å, $\epsilon_{\mathrm{w}} = 0.8$ kJ/mol, and $4\pi\rho = 0.5$ sites/Å^3. These values are based on those for silica. V_{wall} was combined with the atomic Lennard-Jones potentials using Lorentz−Berthelot mixing rules [$\sigma_{ij} = 0.5(\sigma_{ii} + \sigma_{jj})$ and $\epsilon_{ij} = (\epsilon_{ii}\epsilon_{jj})^{1/2}$].

Molecular dynamics (MD) simulations were carried out in the canonical ensemble using the Berendsen thermostat, with an integration time step of 2 fs. The DL-POLY program was used throughout this paper.[24]

Six different interwall distances were explored: 44.9, 36.5, 33.0, 28.0, 26.4, and 24.9 Å. At each gap width, the area of the walls was adjusted so that the average number density of the confined liquid was equal to that of the bulk liquid ($\rho = 0.004$ Å^{-3}). It is important to note that the choice of a constant density ensemble may not be as appropriate as an ensemble of constant chemical potential. However, it is technically much more difficult to perform grand canonical simulations involving insertion and deletion of particles with the present bulky charged species.

To generate well-equilibrated initial configurations, four 600-ps trajectories were initially run for each system at 1000 K. Subsequently, the temperature was lowered in two stages, 600 ps at 600 K and 600 ps at 400 K. Production runs were then performed at 400 K by integrating up to 1.6 ns. All the properties presented in this work and the associated error bars result from averages over those trajectories.

3. Results and Discussion

3.1. Structural Properties. Figures 2 and 3 show the density profiles, $\rho(z)$, expressed in molecules/Å^3 for cations and anions as well as the total particle density at different interwall distances. In the case of cations, the density was calculated from the position of the center of the rings. All the profiles were symmetrized with respect to the middle of the cell.

The total number density (curves without error bars in Figures 2 and 3) shows a clear structure of layers with a high-density peak close to the walls followed by weaker oscillations toward the center of the cell. Such layering behavior is typical of confined fluids and has been observed in many simulations of atomic and molecular liquids.[19,25,26] As the gap was reduced, the total number of layers decreased from seven to four at a gap width of 28.0 Å but then increased again to six as the layers closest to the wall split. Such layer splitting is also shown by the change in the height of the first peaks, comparing panels d and e in Figures 2 and 3. At every gap, cations show higher peaks near the walls, reaching maximum densities twice and even three times (see panel f in Figure 2) that of the bulk value (0.004 Å^{-3}). Anions exhibit shorter, but broader, first maxima (Figure 3), resulting in a very small segregation of cations toward the interface. For the more confined cases, at first glance, it appears that anions segregate toward the walls. However, further analysis shows that the interfacial layer, defined up to the first minimum of $\rho(z)$, has an excess of cations. This can be observed in Figure 4.

Overall, oscillations in the cation density are weaker than those for the anions so that the structure exhibited by the total density at the center of the cell can be attributed to the layering of anions. Also, the evolution of the number of layers is neater for anions, being responsible for the splitting of the total density near the walls.

At this point, it is important to remember that, in the present simulations, changes in the separation between the walls were compensated by changes in the wall area, keeping the mean density constant. Beyond that, the number of cations and anions per unit of area at the interface is a nonmonotonic function of the gap width, as is shown in Figure 4. Both ions exhibit similar trends; a maximum is reached at 28.0 Å as a result of the above-mentioned layer splitting. By inspecting the pair distribution function for ions in the interfacial layers, no evidence of intralayer ordering, stronger than that of the bulk, was found.

Figure 5 shows the pressure on the walls as a function of the gap width *D*. The curve has a maximum at 28 Å, showing the same trends as the concentration of particles at the interface. Such similarity is explained by the short-ranged atom−wall interactions, so that only molecules in the first layer contribute significantly to the average forces. A different behavior could be expected if the surfaces were charged, as is likely to occur in DSSCs under operating conditions. The inset to Figure 5 shows the free-energy changes associated with an isothermal and reversible change of the interwall distance from D_0 to *D*. The transformation is performed at a constant number of particles, so the work done in the process corresponds to the Helmholtz free-energy change,

$$\Delta F(D) = -\int_{D_0}^{D} f_{\mathrm{w}}(z)\,\mathrm{d}z = \Delta U(D) - T\Delta S(D) \qquad (2)$$

where $f_{\mathrm{w}}(z)$ is the average force on the walls and ΔU and ΔS are the associated changes of internal energy and entropy. ΔF and ΔU are directly accessible from the simulations, while the entropic contribution is obtained from the difference.

Since the number of intermediate states simulated in this work may not be enough to allow an accurate evaluation of the former integral, we regard the behavior of the ΔF and $T\Delta S$ curves in the inset to Figure 5 as of qualitative value. With respect to the least-confined situation and across the range of 20 Å of gap widths, the free energy of the liquid increases monotonically. Internal energy changes are always positive, showing a maxi-

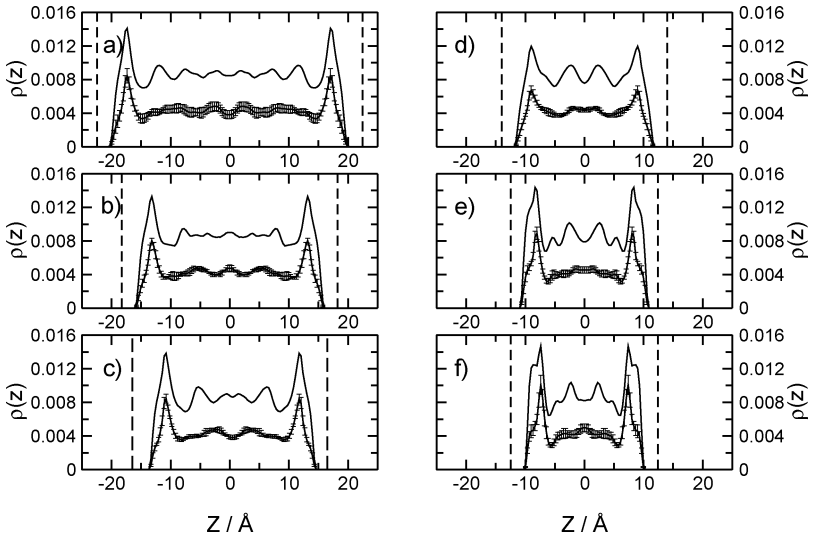

Figure 2. Lines with error bars represent the cation density calculated from the position of the center of the rings. Lines without error bars correspond to the total number density, i.e., the sum of the cation and anion densities ($\rho(z)$ in Å^{-3}). The interwall distances are (a) 44.9, (b) 36.5, (c) 33.0, (d) 28.0, (e) 26.4, and (f) 24.9 Å. The dashed vertical lines show the position of the walls.

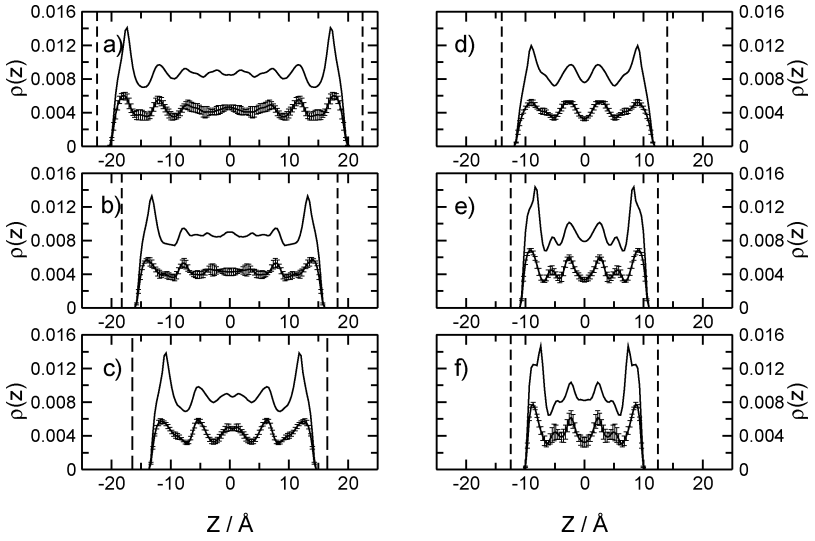

Figure 3. Anion number densities (lines with error bars) for the same interwall distances reported in Figure 2. Lines without error bars correspond to the sum of the cation and anion densities ($\rho(z)$ in Å^{-3}).

mum at 28 Å. Also, by distinguishing Coulombic, van der Waals, and atom−wall contributions, it was clear that the total internal energy change is largely dominated by the intermolecular components, while the average interaction with the walls is always negative. The dominance of the intermolecular contribution in the internal energy changes is related to the distinctive high cohesive energy density of ILs, as compared with that of other polar and nonpolar liquids. At variance with internal energies, entropic changes are negative.

The orientational order as a function of the distance perpendicular to the surfaces was analyzed using the order parameter $P_2(\cos\theta) = \langle(3\cos^2\theta - 1)/2\rangle$, where θ is the angle between a vector fixed in the cation frame and a vector normal to the wall. The brackets denote an average over molecules at position Z and over MD frames. The advantage of using $P_2(\cos\theta)$ is that it takes the value of 0 in the absence of any preferred orientation, while its sign and magnitude give information about the orientations. Figure 6 shows the orientational distributions for (a) a vector normal to the plane of the cation and (b) a vector connecting the two nitrogen atoms. A scaled density profile is also shown in each plot to distinguish regions of enhanced density. It can be seen from the values of P_2 that cations in the

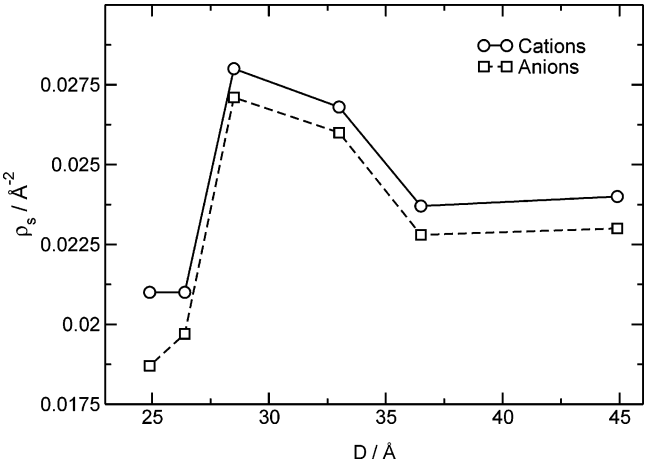

Figure 4. Number of cations (continuous line with circles) and anions (dashed line with squares) in the interfacial layer per unit of surface area as a function of the confinement distance D. The interfacial layer goes between the wall and the first minimum of the total density profile.

contact layer (first density maxima) tend to orient their rings perpendicular to the surface and their N−N axes parallel to the

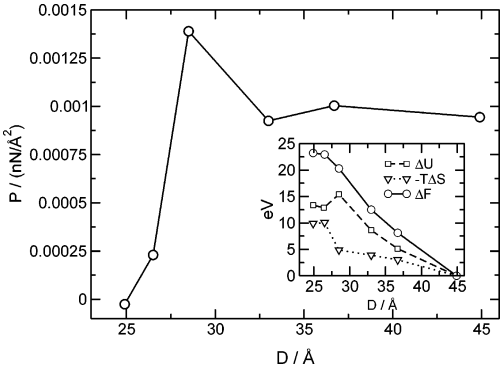

Figure 5. Pressure on the walls as a function of the confinement distance D. Inset: total internal energy change ΔU (squares), $-T\Delta S$ (triangles), and free energies ΔF (circles) as a function of the interwall distance. The reference point is the least-confined system, i.e., $D = 44.9$ Å.

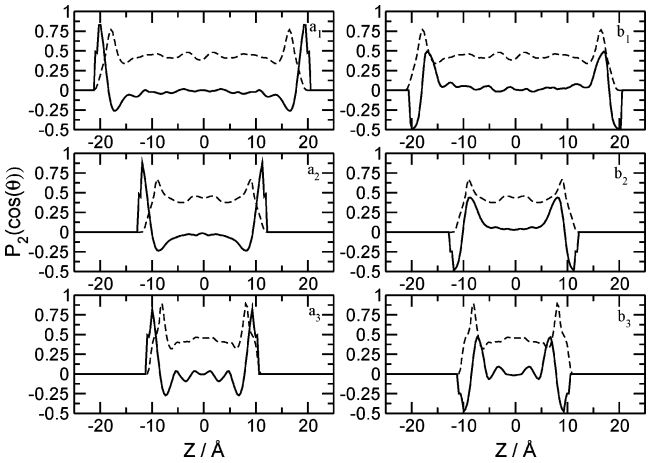

Figure 6. Orientational-order parameter $P_2(\cos\theta)$ along the confinement axis (continuous lines). The dashed lines are scaled cation density profiles. Plots a_1, a_2, and a_3 show the orientation of an axis perpendicular to the cation plane as a function of the interwall distance: $a_1 = 44.9$, $a_2 = 28.0$, and $a_3 = 24.9$ Å. Plots b_1, b_2, and b_3 give the orientation of the vector conecting the two nitrogen atoms.

surface. This is similar to the preferred orientations at the liquid−vapor interface.[27,28] Also, from the values of $P_2 \sim 1$ in plots a_1, a_2, and a_3 of Figure 6, it is clear that, independently of the gap width, there is always a set of cations lying flat on the surface of the walls. However, these ions constitute a small fraction of the contact layer. In the center of the cell any orientational preference is lost, although, in the most confined system, a noticeable second (and even a third) region of oriented molecules becomes apparent, even when the density does not show much structure after the interface.

It is interesting to remark that recent sum-frequency vibrational-spectroscopy experiments on alkyl imidazolium ILs on a silica surface have shown that cations preferentially orient with their planes perpendicular and alkyl groups parallel to the surface normal.[29] Similar results were found at the liquid−gas interface.[30−32] The experimental results pertain to C_4, C_8, C_{12}, and C_{18} alkyl groups. The present results show a similar alignment for the symmetric C_1-substituted imidazolium, [$DMIM^+$], near a smooth wall. This suggests that the orientation of imidazolium cations near a solid surface does not depend on the length of the alkyl substituent. It results from changes in the energetic and entropic balance of the liquid in the vicinity of an interface. Aligning the rings allows a tighter packing and more favorable energy, while the entropy cost is reduced compared to the situation in the bulk as a result of the presence of the interface.

The electrostatic-potential profile determines the force experienced by a test charge moving across the interface. It is, thus, an important factor affecting electronic injection from and to the liquid. Figure 7 shows the potential profiles for different gaps, calculated by integrating the Poisson's equation for the total charge densities. Clearly, there is an average potential drop between a point inside the walls (taken as reference) and the center of the confined liquid of around −0.5 V. However, in all the cases, the potential oscillates strongly into the bulk. By comparing the charge distributions calculated from the charge on every atom in the system with those obtained by assigning the total ionic charge to the center of the molecules, it resulted that the total charge density follows from the arrangement of the ions but with an important contribution arising from the orientation of the cations. This orientational contribution is expected from the trends in the order parameters, P_2 of Figure 6, and has more weight in the most confined systems.

3.2. Dynamical Properties. The diffusion of molecules in a confined liquid is known to be different from that of the bulk fluid. In particular, oscillations in the diffusion coefficients of simple liquids, as a function of the confinement distance, have been reported by Gao et al.[26] Within the context of DSSCs, the motion of the ions through the interstitial space left by the semiconductor network is essential to maintain a sustained electric current.

The mean-square displacements of the ions were calculated and discriminated according to the motions perpendicular and parallel to the walls. Diffusion coefficients were obtained from the slope of the mean-square displacements for delay times longer than 1 ns; averaging over four independent MD trajectories. Figure 8 shows the global-diffusion coefficient D_{xx} for motions along the $X-Y$ plane (by symmetry $D_{xx} = D_{yy}$) for both cations and anions at different gap widths. The first feature to notice is the higher diffusivity of cations, for all interwall distances. This is also observed in the simulation of the bulk system as well as in classical simulations of many other ILs.[13,22,33,34] The second feature is that, except for the most confined situation, ions move faster under confinement than in the bulk liquid, whose values of D_{xx} are indicated by arrows on the right axis.

By comparing the mobility parallel and perpendicular to the surface, it was clear that both ions diffuse faster on the $X-Y$ plane than in the perpendicular direction. It was also found that those ions that remain close to the walls during a complete simulation diffuse faster than the average ions, a fact possibly related to the lack of corrugation of the walls that allows ions to slide more easily on the $X-Y$ plane. In addition, the solvophobic nature of the walls may also be a contributing factor. The maxima in the diffusion coefficients as a function of the gap width reflect the maxima in the proportion of ions close to the walls, observed in Figure 4, and the variations in the height of the first density peaks in Figures 2 and 3. The resulting behavior arises from the combined effect of compression and increment in the surface area, as is explained below.

The total cation and anion diffusion coefficients averaged over all the particles, reported in Figure 8, contain contributions from particles far from and near the walls. Ions close to the walls diffuse faster than those in the center. In a first approximation, the latter can be considered as bulk particles. The number of ions, N_c, at the interface is given by $N_c = S\int_a^b \rho(z)\,dz$, where S is the area of the wall, a is a point inside the wall where the

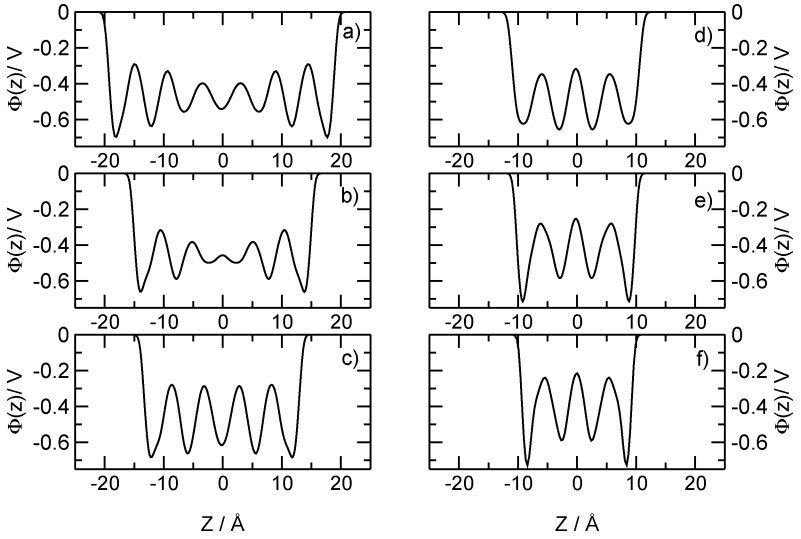

Figure 7. Electrostatic-potential profiles (in V) for the same confinement distances reported in Figures 2 and 3.

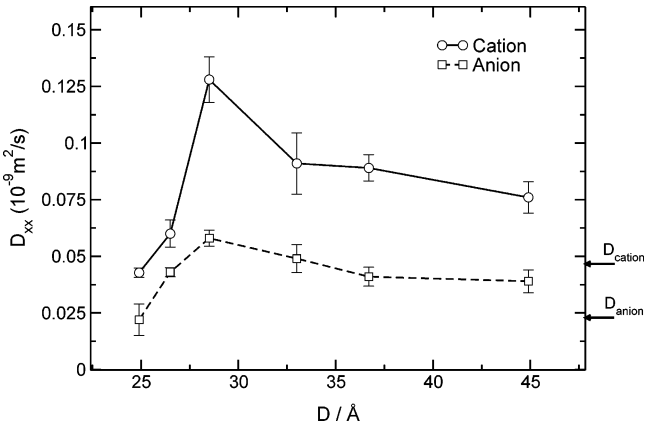

Figure 8. Cation (solid line with circles) and anion (dashed line with squares) diffusion coefficients, D_{xx}, in the $X-Y$ plane as a function of the confinement distance D. The arrows on the right axis indicate the bulk values.

density is negligible, and b is the first minimum of the density profile $\rho(z)$. Increasing S while keeping constant the total number of particles introduces a simple geometric effect on the total diffusion coefficient. However, the nonmonotonic behavior of the curves in Figure 8 arises from changes in N_c associated with variations in the thickness ($b - a$) and density of the interface layer. It is expected that, locally, the diffusivity decreases with increasing density. This behavior can indeed be observed in the present simulations by comparing the height of the first density peak at different wall separations. This height is at a minimum at 28 Å, precisely where the total diffusion coefficient exhibits a maximum.

It is important to remark that, at all the interwall distances explored, the molten salt preserved a liquid behavior and no "hardening" or transition to a solidlike structure was observed. This trend is different to that reported by Gao et al.[26] for an atomic fluid between corrugated walls, where evidence of a confinement-induced transition to a solidlike phase was observed. In this case, the diffusion coefficient decreased in an oscillatory way with respect to the bulk value.

The preservation of the liquid behavior of the molten salt may not necessarily be a consequence of the lack of roughness of the walls but, instead, the result of a particular balance of interactions between the molecules and between the molecules and the wall.

4. Conclusions

Using MD simulations, we have studied the behavior of the IL [DMIM][Cl] confined between two parallel structureless walls. The simulations attempt to model the environment experienced by the ions in the pores of the semiconductor layer of a DSSC.

Density profiles perpendicular to the walls show an interfacial liquid layer twice as dense as the bulk followed by oscillations that decay toward the center of the cell. It is also clear that a major part of the layering is due to the distribution of anions. The number of layers changes with the interwall distance and so does the concentration of ions at the interface, showing a maximum at 28 Å. The observed structural effects result from the response of the liquid to the boundary conditions imposed and are detected also in the pressure on the walls. The pressure is determined by the number of particles in the first density layer, a result of the short-range interactions between the atoms and the walls. This effect is expected to depend on the details of the ion−wall interactions and may be significantly different in the case of charged surfaces.

The analysis of the orientational order parameter, $P_2(\cos\theta)$, in conjunction with the density profiles, indicates that cations at the interface orient their planes tilted with respect to the surface. This is a result that, in light of recent experimental findings,[29] may be independent of the type of confining walls used in the present simulations.

The distribution of charge perpendicular to the surface is determined by the arrangement of the ions and, in particular, by the alignment of the cations. As a result, any test charge entering the liquid will encounter a first layer of positive charge followed by a second layer of opposite sign. The electrostatic-potential drop between a point inside the walls and the middle of the liquid slab is around −0.5 V, although the potential oscillates strongly into the liquid.

An interesting result is that, under confinement, ionic diffusion is faster than in the bulk, at least in the presence of noncorrugated walls. Ions close to the surfaces diffuse faster than those in the middle of the slab, so the diffusion coefficients reflect the changes in the density and proportion of ions near the walls. The reasons for the faster diffusion near the walls may be related to their lack of corrugation, their solvophobic nature, or a combination of both. However, it must also be kept in mind that the local mobility depends on the local density

and orientation of the ions, which are the result of collective structural effects.

If the observed trends in ionic mobility apply also to more realistic surfaces, then the higher diffusivity of the ions will surely have an impact on the electrical conductivity and response of the IL to internal electric field changes. In fact, it has been proposed that the ability of the liquid to screen, fast and efficiently, an external field controls the rate of charge-carrier percolation across the nanocrystalline film in DSSCs.[1]

There are several aspects of ILs that need further attention in connection with their uses in solar cells. First, a more realistic modeling of the walls would be necessary as well as the consideration of more sophisticated ILs. Second, it is important to understand the dynamical response of the semiconductor/IL interface to changes in the surface charge. The exploration of some of these issues is underway.

Acknowledgment. We would like to thank C. Hardacre, T. Youngs, and A. Walker for fruitful discussions. This work was funded by the Engineering and Physical Sciences Research Council (EPSRC) of the U.K., Grant GR/S41562. R.M.L.-B. thanks the Leverhulm Trust for an emeritus fellowship.

References and Notes

(1) Grätzel, M. *Nature* **2001**, *414*, 338−344.
(2) Grätzel, M. *J. Photochem. Photobiol., C* **2003**, *4*, 145−153.
(3) Grätzel, M. *J. Photochem. Photobiol., A* **2004**, *164*, 3−14.
(4) Hagfeldt, A.; Grätzel, M. *Chem. Rev.* **2000**, *33*, 269−277.
(5) Hagfeldt, A.; Grätzel, M. *Acc. Chem. Res.* **2000**, *33*, 269−277.
(6) Mora-Seró, I.; Bisquert, J. *Nano Lett.* **2003**, *3*, 945−949.
(7) Eppler, A. M.; Ballard, I. M.; Nelson, J. *Physica E* **2002**, 197−202.
(8) Wolfbauer, G.; Bond, A.; Eklund, J. C.; Macfarlane, D. *Sol. Energy Mater. Sol. Cells* **2001**, *70*, 85−101.
(9) Hara, K.; Nishikawa, T.; Kurashige, M.; Kawauchi, H.; Kashima, T.; Sayama, K.; Aika, K.; Arakawa, H. *J. Phys. Chem. B* **2002**, *106*, 12693−12704.
(10) Kawano, R.; Watanabe, M. *Chem. Commun.* **2003**, *3*, 330−331.
(11) Rogers, R. D., Seddon, K. R., Volkov, S., Eds. *Green Industrial Applications of Ionic Liquids*; NATO Science Series; Kluwer Academic Publishers: Boston, 2002.
(12) Wasserscheid, P., Welton, T., Eds. *Ionic Liquids in Synthesis*; Wiley−VCH: Weinheim, 2002.
(13) Del Pópolo, M. G.; Voth, G. A. *J. Phys. Chem. B* **2004**, *108*, 1744−1752.
(14) Hanke, C. G.; Price, S. L.; Lynden-Bell, R. M. *Mol. Phys.* **2001**, *10*, 801−809.
(15) Clifford, J. N.; Palomares, E.; Nazeeruddin, M. K.; Grätzel, M.; Nelson, J.; Li, X.; Long, J.; Durrant, J. *J. Am. Chem. Soc.* **2004**, *126*, 5225−5233.
(16) Schlichthörl, G.; Huang, S.; Sprague, J.; Frank, A. J. *J. Phys. Chem. B* **1997**, *101*, 8141−8155.
(17) Barbé, C.; Arendse, F.; Comte, P.; Jirousek, M.; Lenzmann, F.; Shklover, V.; Grätzel, M. *J. Am. Ceram. Soc.* **1997**, *80*, 3157−3171.
(18) Camará, L.; Bresme, F. *J. Chem. Phys.* **2003**, *119*, 2792−2800.
(19) Senapati, S.; Chandra, A. *Chem. Phys.* **1998**, *231*, 65−80.
(20) Schoen, M.; Diestler, D. *Phys. Rev. E* **1997**, *56*, 4427−4440.
(21) Du, Q.; Superfine, R.; Freysz, E.; Shen, Y. R. *Phys. Rev. Lett.* **1993**, *70*, 2313−2316.
(22) de Andrade, J.; Böes, E.; Stassen, H. *J. Phys. Chem. B* **2002**, *106*, 13344−13351.
(23) Nicholson, D.; Parsonage, N. G. *Computer Simulation and the Statistical Mechanics of Adsorption*; Academic Press: New York, 1982.
(24) Smith, W.; Forester, T. R. The DL_POLY Molecular Simulation Package; http://www.dl.ac.uk/TCSC/Software/DL_POLY/main.html, 1999 (reference manual).
(25) Gao, J.; Luedtke, W. D.; Landman, U. *J. Phys. Chem. B* **1997**, *101*, 4013−4023.
(26) Gao, J.; Luedtke, W. D.; Landman, U. *Phys. Rev. Lett.* **1997**, *79*, 705−708.
(27) Lynden-Bell, R. M. *Mol. Phys.* **2003**, *101*, 2625−2633.
(28) Lynden-Bell, R. M.; Kohanoff, J.; Del Pópolo, M. G. *Faraday Discuss.* **2005**, *129*, 57−67.
(29) Fitchett, B. D.; Conboy, J. *J. Phys. Chem. B* **2004**, *108*, 20255−20262.
(30) Gannon, T. G.; Law, G.; Watson, P. R.; Carmichael, A. J.; Seddon, K. R. *Langmuir* **1999**, *15*, 8429−8434.
(31) Law, G.; Watson, P.; Carmichael, A. J.; Seddon, K. R. *Phys. Chem. Chem. Phys.* **2001**, *3*, 2879−2885.
(32) Carmichael, A. J.; Hardacre, C.; Holbrey, J. D.; Nieuwenhuyzen, M.; Seddon, K. R. *Mol. Phys.* **2001**, *99*, 795−800.
(33) Margulis, C. J.; Stern, H. A.; Berne, B. J. *J. Phys. Chem. B* **2002**, *106*, 12017−12021.
(34) Liu, Z.; Huang, S.; Wang, W. *J. Phys. Chem. B* **2004**, *108*, 12978−12989.